

# The stellar content of the Hamburg/ESO survey<sup>★</sup>

## IV. Selection of candidate metal-poor stars

N. Christlieb<sup>1,2</sup>, T. Schörck<sup>2</sup>, A. Frebel<sup>3</sup>, T.C. Beers<sup>4</sup>, L. Wisotzki<sup>5</sup>, and D. Reimers<sup>2</sup>

<sup>1</sup> Department of Astronomy and Space Physics, Uppsala University, Box 515, 75120 Uppsala, Sweden  
e-mail: norbert@astro.uu.se

<sup>2</sup> Hamburger Sternwarte, Universität Hamburg, Gojenbergsweg 112, D-21029 Hamburg, Germany  
e-mail: nchristlieb/dreimers@hs.uni-hamburg.de

<sup>3</sup> McDonald Observatory, The University of Texas at Austin, 1 University Station, C1400, Austin, TX 78712-0259  
e-mail: anna@astro.as.utexas.edu

<sup>4</sup> Department of Physics and Astronomy, CSCE: Center for the Study of Cosmic Evolution, and JINA: Joint Institute for Nuclear Astrophysics, Michigan State University, E. Lansing, MI 48824, USA  
e-mail: beers@pa.msu.edu

<sup>5</sup> Astrophysical Institute Potsdam, An der Sternwarte 16, D-14482 Potsdam, Germany  
e-mail: lutz@aip.de

Received 28 September 2007 / Accepted 4 March 2008

### ABSTRACT

We present the quantitative methods used for selecting candidate metal-poor stars in the Hamburg/ESO objective-prism survey (HES). The selection is based on the strength of the Ca II K line,  $B - V$  colors (both measured directly from the digital HES spectra), as well as  $J - K$  colors from the 2 Micron All Sky Survey. The KP index for Ca II K can be measured from the HES spectra with an accuracy of 1.0 Å, and a calibration of the HES  $B - V$  colors, using CCD photometry, yields a 1- $\sigma$  uncertainty of 0.07 mag for stars in the color range  $0.3 < B - V < 1.4$ . These accuracies make it possible to reliably reject stars with  $[\text{Fe}/\text{H}] > -2.0$  without sacrificing completeness at the lowest metallicities. A test of the selection using 1121 stars of the HK survey of Beers, Preston, and Shectman present on HES plates suggests that the completeness at  $[\text{Fe}/\text{H}] < -3.5$  is close to 100 % and that, at the same time, the contamination of the candidate sample with false positives is low: 50 % of all stars with  $[\text{Fe}/\text{H}] > -2.5$  and 97 % of all stars with  $[\text{Fe}/\text{H}] > -2.0$  are rejected. The selection was applied to 379 HES fields, covering a nominal area of 8853 deg<sup>2</sup> of the southern high Galactic latitude sky. The candidate sample consists of 20,271 stars in the magnitude range  $10 \leq B \leq 18$ . A comparison of the magnitude distribution with that of the HK survey shows that the magnitude limit of the HES sample is about 2 mag fainter. Taking the overlap of the sky areas covered by both surveys into account, it follows that the survey volume for metal-poor stars has been increased by the HES by about a factor of 10 with respect to the HK survey. We have already identified several very rare objects with the HES, including, e.g., the three most heavy-element deficient stars currently known.

**Key words.** stars: metal-poor – Surveys

## 1. Introduction

The chemical abundances of the atmospheres of metal-poor stars preserve, to a large extent, the chemical composition of the gas clouds from which they formed. Therefore, metal-poor (and thus old) stars provide an observational channel through which we can study the early history of the Galaxy and the Universe. These stars can be used, e.g., for determining a lower limit for the age of the Universe, estimating the amount of <sup>7</sup>Li produced in Big Bang Nucleosynthesis, or constraining the elemental yields of the first generations of supernovae (SNe). Details on these and other topics relevant to the uses of metal-poor stars can be found in the review by Beers & Christlieb (2005).

Send offprint requests to: N. Christlieb,  
e-mail: norbert@astro.uu.se

<sup>★</sup> Based on observations collected at the European Southern Observatory, Chile (Proposal ID 145.B-0009). Tables A.1 and A.2 are only available in electronic form at the CDS via anonymous ftp to cdsarc.u-strasbg.fr (130.79.125.5) or via http://cdsweb.u-strasbg.fr/Abstract.html.

The Hamburg/ESO objective-prism Survey (HES) was originally conceived for finding bright quasars (Reimers 1990; Wisotzki et al. 1996, 2000). It was carried out as an ESO Key Program (proposal 145.B-0009; P.I.: D. Reimers). For details of the concept behind the survey and the data processing, we refer the interested reader to Wisotzki et al. (2000). The data quality of the HES offered an efficient means of exploiting the stellar content of the survey. In previous papers of this series, we reported on searches for DA white dwarfs (Christlieb et al. 2001b; Paper I), high-latitude carbon stars (Christlieb et al. 2001a; Paper II), and field horizontal-branch stars (Christlieb et al. 2005; Paper III). In this paper we describe quantitative methods for selecting candidates for very metal-poor stars (i.e., stars at  $[\text{Fe}/\text{H}] < -2.5$ ) in the HES database of digital objective-prism spectra.

After a brief description of the HES (Sect. 2) we present calibrations of line indices, an improved calibration of  $B - V$  colors estimated directly from the HES spectra (Sect. 3). The quantitative criteria that were applied to the digital HES spectra for selecting metal-poor candidates, as well as the visual inspection

procedure for the selected candidates, are described in Sect. 4. An evaluation of the selection is presented in Sect. 5. In Sect. 6 we report on some of the basic properties of the metal-poor candidate sample, including the magnitude distribution, before we present our conclusions in Sect. 7.

Results of spectroscopic follow-up observations of the candidates will be presented in forthcoming papers. However, the results for bright candidates from 329 HES plates have already been reported in Frebel et al. (2006b), and the results for fainter stars have occasionally been published in papers focusing on abundance analyses of HES metal-poor stars based on high-resolution spectroscopy (see Sect. 2.3 for references). We note that CCD photometry for many of the most interesting metal-poor candidates has already been published in Beers et al. (2007).

## 2. The Hamburg/ESO Survey

### 2.1. Basic survey properties

The HES is based on photographic plates taken with the 1 m ESO Schmidt telescope, using its  $4^\circ$  prism. The 379 HES fields cover a total nominal area of  $8853 \text{ deg}^2$  of the southern high Galactic latitude sky. Taking overlapping plates and plate quarters as well as losses in area due to overlapping spectra into account, the effective survey area is  $6726 \text{ deg}^2$ . The plates have been scanned at Hamburger Sternwarte with a PDS microdensitometer. The large physical size of the ESO Schmidt plates required that each plate be scanned in four separate sections, so that the full matrix scans of each HES plate consists of four parts of  $7500 \times 7500$  pixels each.

The input catalog for extracting the HES spectra was generated from direct images of the Digitized Sky Survey-I (DSS-I).<sup>1</sup> Each of the objects in the input catalog was assigned to one of the following three object classes: unsaturated point sources (source type “stars”), bright sources above a saturation threshold determined by examining the characteristic curve of each individual HES plate (“bright”), and objects that have been classified as extended sources by an automated morphological classification based on the DSS-I images (“ext”). Note that the last class of sources does not exclusively consist of galaxies and other objects that are indeed extended, but also point-like sources located in the diffraction spikes of very bright stars, or pairs of objects located very close to one another that are not separated on the DSS-I direct image.

A photometric calibration of the HES was established through photometric sequences obtained for all fields, mainly in the course of the Reimers et al. ESO Key Program, and augmented by sequences taken from the latest version of the *Guide Star Photometric Catalog 2* (Bucciarelli et al. 2001). The overall  $1-\sigma$  accuracy, including zero point errors, is better than 0.15 mag in  $B_J$  in the majority of the fields, degrading to 0.20 mag in a few fields in which only sequences of lower quality are available.

<sup>1</sup> The DSS-I is based on photographic data obtained using The UK Schmidt Telescope. The UK Schmidt Telescope was operated by the Royal Observatory Edinburgh, with funding from the UK Science and Engineering Research Council, until 1988 June, and thereafter by the Anglo-Australian Observatory. Original plate material is copyright (c) the Royal Observatory Edinburgh and the Anglo-Australian Observatory. The plates were processed into the present compressed digital form with their permission. The Digitized Sky Survey was produced at the Space Telescope Science Institute under US Government grant NAG W-2166.

An astrometric transformation between the DSS-I and HES plates was determined, yielding for each object in the input catalog the  $x, y$  position on the HES plate used for extracting its spectrum in the sky-background reduced HES plate scan. The HES spectra are extracted by algorithms optimized for each of the above mentioned source types (see Wisotzki et al. 2000 for details). The HES data base consists of 12,357,153 digital spectra extracted on 379 plates. This data base, as well as the full-matrix HES plate scans, will be made available online in the near future.

The wavelength coverage of the HES spectra is limited by the atmospheric cutoff at the blue end, and the sharp sensitivity cutoff of the IIIa-J emulsion (“red edge”), resulting in a wavelength range of  $3200 \text{ \AA} < \lambda < 5300 \text{ \AA}$  (see Fig. 1). The spectral resolution of the HES is mainly seeing-limited; it is typically  $\Delta\lambda = 10 \text{ \AA}$  at the location of the Ca II K line, at  $\lambda = 3934 \text{ \AA}$ .

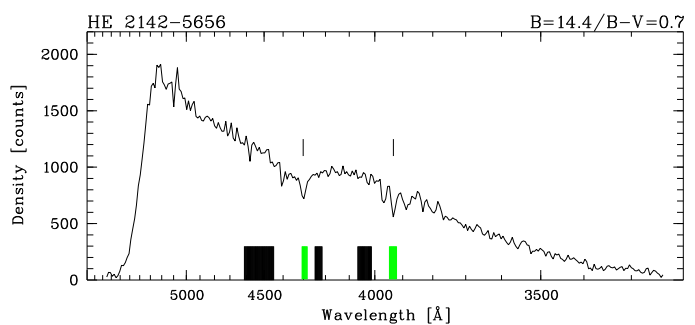


**Fig. 1.** HES example spectrum. The positions of the G band of CH and the Ca II K lines are marked, and the wavelength regions of the continuum (black) and line (grey) passbands for the measurement of the GP and KP indices are indicated.

The quality of the HES spectra make this survey well-suited for executing a search for metal-poor stars. In particular, as can be seen in Fig. 8, the spectral resolution is sufficient to detect the Ca II K line even in quite metal-poor stars. This line can be used as an indicator for  $[\text{Fe}/\text{H}]$ , since for the overwhelming majority of the stars in the Galaxy, the abundance ratio  $[\text{Ca}/\text{Fe}]$  follows a well-defined trend. The spectral coverage of the HES spectra is broad enough to provide some color information directly from the objective-prism spectra. Even though the V band is not fully covered by the HES spectra, there is a strong correlation between a so-called “half power point” – a bisecting point of the photographic density distribution in an appropriate wavelength range (see Fig. 7 of Christlieb et al. 2001b for an illustration) – and the  $B - V$  color. Christlieb et al. (2001b) showed that this correlation can be used to estimate  $B - V$  colors directly from the HES spectra with an accuracy of  $\sim 0.1$  mag. Color information is important for avoiding a bias against cool metal-poor giants, which would occur if the stars were selected based only on their Ca II K line strength, because in cool giants this line has a considerable strength even if the stars are metal poor.

With a limiting magnitude for stellar work of  $B \sim 17.5$ , another advantage of the HES is that it is  $\sim 2$  mag deeper than the previously largest survey for metal-poor stars, the so-called HK survey of Beers, Preston, and Shectman (Beers et al. 1985, 1992). Taking the overlap in area of the HK and HE surveys into account, it follows that with the HES, the total survey volume for metal-poor stars is increased by about a factor of  $\sim 10$  with respect to the HK survey alone.

## 2.2. Follow-up spectroscopy of metal-poor candidates

As a result of the increased survey volume, the ongoing spectroscopic follow-up observations of candidate metal-poor stars identified in the HES have led to the discovery of stars that could not have been found in previous surveys, due to their extreme rarity. For example, the three most heavy-element deficient stars currently known were found in the HES: HE 1327–2326 ([Fe/H] =  $-5.4$ ; Frebel et al. 2005; Aoki et al. 2006; Frebel et al. 2006a)<sup>2</sup>; HE 0107–5240 ([Fe/H] =  $-5.7$ ; Christlieb et al. 2002, 2004b; Bessell et al. 2004; Christlieb et al. 2008); and HE 0557–4840 ([Fe/H] =  $-4.7$ ; Norris et al. 2007). That is, some 20 years after Bessell & Norris (1984) discovered the extremely metal-poor giant CD  $-38^\circ 245$ , with [Fe/H]  $\sim -4.0$  (Norris et al. 2000; François et al. 2003), it is now possible to study, by means of long-lived stars, the history of our Galaxy when it was enriched by heavy-elements to a level of only [Fe/H]  $\sim -5.0$ , corresponding to redshifts of  $z > 5$  (Clarke & Bromm 2003). It can be expected that new, even deeper surveys for metal-poor stars, such as SEGUE: The Sloan Extension for Galactic Understanding and Exploration<sup>3</sup>, will yield significant numbers of additional stars in this [Fe/H] range. A review of past, present, and future metal-poor star surveys can be found in Beers & Christlieb (2005).

## 2.3. High-resolution spectroscopy of confirmed metal-poor stars

In addition to the objects mentioned in the previous section, many confirmed metal-poor stars from the HES have already been observed at high spectral resolution (i.e.,  $R = \lambda/\Delta\lambda \geq 40,000$ ). The spectra were obtained at 8 m-class telescopes, including Keck-I (Cohen et al. 2002; Carretta et al. 2002; Lucatello et al. 2003; Cohen et al. 2003, 2004, 2005, 2006), VLT-UT2 (Depagne et al. 2000; Frebel et al. 2007a), Subaru (Goswami et al. 2006; Frebel et al. 2007b; Aoki et al. 2007), and Magellan-I.

A dedicated observational program for identifying metal-poor stars that are strongly enhanced in r-process elements, the Hamburg/ESO R-process Enhanced star Survey (HERES; Christlieb et al. 2004a), has also been carried out with the VLT. So-called “snapshot spectra” (i.e., spectra with  $R \sim 20,000$  and  $S/N \sim 50$  per pixel) of 373 metal-poor stars, of which 346 stem from the HES, were obtained with VLT/UVES. Barklem et al. (2005) report on the results of an automated and homogeneous abundance analysis of 253 stars whose spectra are not heavily contaminated with CH lines. The carbon and nitrogen abundances of 94 HERES stars, including 72 stars not analyzed by Barklem et al. (2005) because of their strong CH lines, were determined by Lucatello et al. (2006). They also discuss the frequency of carbon-enhanced stars among metal-poor stars, based on the HERES sample. Hayek et al. (2008) present a detailed abundance analysis of the strongly r-process enhanced star HE 1219–0312 (and an additional such star, CS 29491–069, from the HK survey), and Jonsell et al. (2006) report on an analysis of HE 0338–3945, a star enriched in r- and s-process elements. Additional HERES papers are in preparation.

A sample of 1777 bright (i.e.,  $9 < B < 14$ ) metal-poor candidates selected on 329 HES plates has been presented by Frebel et al. (2006b). HE 1327–2326 ( $B = 14.016$ ;

Aoki et al. 2006) is a member of this group of HES stars, as is HE 1523–0901, a bright ( $B = 12.186$ ; Beers et al. 2007), strongly r-process enhanced ([r/Fe] =  $+1.8$ ) star in which the U II line at  $\lambda = 3859.57 \text{ \AA}$  is detected (Frebel et al. 2007a), which is crucial for determining a nucleochronometric age of a star. Snapshot spectra of confirmed metal-poor stars from this sample have been obtained with the AAT/UCLES, Magellan/MIKE, VLT/UVES, and HET/HRS.

The selection described in this paper includes bright stars, thus many of the stars already published in Frebel et al. (2006b) are also present in the sample reported herein. However, the selection criteria for bright stars have been improved compared to those of Frebel et al.; in particular, we only make limited use of the HES  $B - V$  colors for bright stars, because this color has been shown by Frebel et al. to be unreliable due to saturation effects for objects brighter than  $B = 13$ . Instead, we now use a selection criterion based on  $J - K$  colors from the Two Micron All Sky Survey (2MASS; Skrutskie et al. 2006); i.e., a criterion which does not involve any colors measured from HES spectra. We also extended the selection of bright stars to 50 HES fields that were not explored by Frebel et al.

## 3. Calibrations

As explained in Sect. 2.1 above, we wish to make use of the  $B - V$  or  $J - K$  color and the strength of the Ca II K line to perform a quantitative, bias-free selection of metal-poor candidates in the HES. Over a wide color range, the Ca II K line is strong enough to be detected even at low metallicities, and at a given color, the KP index typically varies by more than  $2 \text{ \AA}$  per dex in [Fe/H] (see Fig. 5), making a selection based on these observables feasible. While  $J$  and  $K$  photometry is available from 2MASS, the  $B - V$  color and the KP index can be measured directly from the HES spectra. However, it is necessary to calibrate these measurements against CCD photometry and previously obtained medium-resolution spectra, respectively, to avoid systematic offsets in the HES measurements.

### 3.1. $B - V$ color

Observations with a Schmidt telescope and an objective prism yield slitless spectroscopy, from which approximate spectrophotometric information can be extracted. In the case of the HES, the plate material is sufficiently homogeneous (as judged from the results presented at the end of this section), and the wavelength range, covering the full  $U$  and  $B$  bands, as well as about half of the  $V$  band, is large enough to extract color information directly from the digital objective-prism spectra. Wisotzki et al. (2000) defined so-called spectral half-power points (HPPs) of HES spectra for selecting quasar candidates by means of their spectral energy distribution. Christlieb et al. (2001b) calibrated two of these HPPs onto the  $UBV$  photometric system, yielding estimates of  $U - B$  and  $B - V$  for all HES sources. The Christlieb et al. (2001b) calibration for  $B - V$  reached an accuracy of 0.1 mag in the color range  $-0.6 < B - V < 2.0$ . We slightly improve on that accuracy by establishing a calibration for  $B - V$  which is restricted to the color range relevant for selecting metal-poor candidates, i.e.,  $0.3 < B - V < 1.4$ .

To carry out this calibration, we employ 1039 metal-poor stars from the HK survey in the magnitude range  $12 < B < 16$  that are also present on HES plates, and for which accurate CCD photometry is available. Excluded from the calibration sample (as well as from the selection of metal-poor stars) were stars

<sup>2</sup>  $[X/H] = \log_{10} [N(X)/N(H)]_* - \log_{10} [N(X)/N(H)]_\odot$ , and analogously for  $[X/Fe]$ .  $N(X)$  is the number density of atoms of the element  $X$ .

<sup>3</sup> [www.sdss.org/segue](http://www.sdss.org/segue)

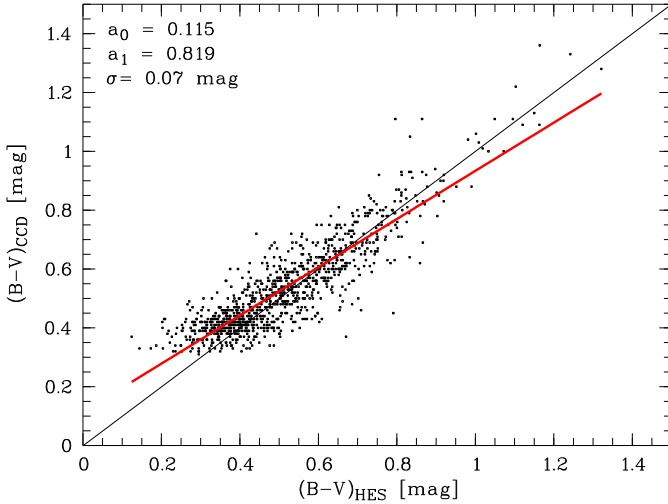


**Fig. 2.** Calibration of  $B - V$  colors estimated from HES spectra, using 1039 metal-poor stars from the HK survey present on HES plates.

which have been detected in the HES as being influenced by an overlapping spectrum caused by an object in the dispersion direction (hereafter referred to as *overlaps*). The calibration sample includes 625 stars (i.e., unsaturated point sources), 338 sources of the object type *bright* (i.e., sources above a saturation threshold), and 76 *ext* objects (i.e., objects that have been classified as extended sources).

Figure 2 shows the result of the  $B - V$  calibration exercise for the sample of 1039 HK-survey stars. The  $1-\sigma$  uncertainty is 0.07 mag. This is remarkably low for colors estimated from photographic plates, especially considering that the calibration involves stars from many plates, taken over a period of almost 10 years. Calibrating all three classes of sources separately yielded  $1-\sigma$  uncertainties of 0.06 mag (*stars*), 0.07 mag (*bright*), and 0.08 mag (*ext*), respectively. We use these individual calibrations for the respective source types for selecting metal-poor candidates, whereas *ext* sources are excluded from the selection altogether to avoid galaxies entering the candidate sample as false positives.

### 3.2. Line indices

Line indices compare the continuum level at the center of an absorption line or feature with its depth relative to the continuum. Indices are a measure of the integrated absorption of the line or feature, and, analogous to equivalent widths, they carry units of wavelengths. Beers et al. (1999) defined the KP index for the Ca II K line, and the GP index for the CH G band. We calibrated these indices obtained from HES spectra, by comparing with measurements of these indices in medium-resolution (i.e.,  $\Delta\lambda \sim 2 \text{ \AA}$ ) spectra of more than 2000 HK-survey stars present on HES plates. The wavelength bands of the indices, as used in the HES, are summarized and compared to the Beers et al. (1999) definitions in Tab. 1, and illustrated in Fig. 1.

#### 3.2.1. The KP index

Since the resolution of the HES spectra is typically  $10 \text{ \AA}$  at Ca II K (depending on the seeing), the spectral lines are broadened to an extent where essentially no continuum is present between H $\delta$  and Ca II K. Therefore, it was not possible to use the

**Table 1.** Wavelength bands of the KP index for the Ca K line and the GP index for the G band of CH, as employed in the HES (KPHES, GPHES), and compared with the definitions of K6, K12, K18 and GP of Beers et al. (1999).

Index	Blue Sideband [Å]	Line Band [Å]	Red Sideband [Å]
KPHES	—	3920.0–3946.0	4011.0–4065.0
K6	3903.0–3923.0	3930.7–3936.7	4000.0–4020.0
K12	3903.0–3923.0	3927.7–3939.7	4000.0–4020.0
K18	3903.0–3923.0	3924.7–3942.7	4000.0–4020.0
GPHES	4246.0–4255.0	4281.0–4307.0	4446.0–4612.0
GP	4247.0–4267.0	4297.5–4312.5	4362.0–4372.0

blue sideband for the KP index defined by Beers et al. (1999), or any other blue sideband, for that matter. For the same reason, the red sideband employed by Beers et al. was replaced by a  $54 \text{ \AA}$  wide band covering the wavelength region  $4011\text{--}4065 \text{ \AA}$ .

The resolution of the HES spectra does not allow one to distinguish between the  $6 \text{ \AA}$ ,  $12 \text{ \AA}$ , and  $18 \text{ \AA}$  wide line bands for the Ca II K line defined by Beers et al. (1999). We therefore do not apply the band-switching scheme for the line passband suggested by Beers et al. Instead, a single  $26 \text{ \AA}$  wide band centered on Ca II K was used. This band is sampled by only 4 pixels in the HES spectra.

We proceed by fitting a second-order polynomial to the data points from the HES KP measurements (hereafter KPHES) and those from the medium-resolution follow-up spectra (hereafter KPfu), after rejecting 104 stars as  $> 2\sigma$  outliers in a first iteration of the fit (see Fig. 3), leaving 2162 stars. In Fig. 3 one can see a distinct group of 53 stars (i.e.,  $\sim 2\%$  of the sample of calibration stars) with KPHES in the range  $8\text{--}15 \text{ \AA}$  and KPfu  $< 5 \text{ \AA}$ . Inspection of the HES spectra reveals that these are spectra of cool stars affected by strong molecular features bluewards of the Ca K line. As has been shown by Cohen et al. (2005), the presence of CH and CN lines in the continuum bands used for the measurement of the KP index leads to systematically too low KP index values. In Fig. 2 of Cohen et al. (2005) it can be seen that the blue continuum band is more strongly affected by the CH and CN lines than is the red continuum band, and since the blue continuum band is not used in the HES, a systematic offset between KPHES and KPfu results.

The  $1-\sigma$  scatter of KPHES around the adopted calibration relation is  $1.0 \text{ \AA}$ . Reading from panel *a* of Fig. 5, this translates into uncertainties in  $[\text{Fe}/\text{H}]$  of about  $1.0/0.5/0.2/0.3 \text{ dex}$  at  $(B - V)_0 = 0.3/0.4/0.7/1.0$ , respectively. The uncertainties in  $[\text{Fe}/\text{H}]$  due to errors in  $(B - V)_0$  are negligible compared to those caused by the errors in KP. For faint or very bright HES stars, the uncertainties in  $[\text{Fe}/\text{H}]$  are higher by up to a factor of about 2, since the errors in KP are larger than  $1.0 \text{ \AA}$  (see Fig. 6). However, the numbers listed above indicate that for cool giants in the magnitude range  $B \sim 13\text{--}16$ ,  $[\text{Fe}/\text{H}]$  can be estimated from HES spectra with an accuracy that is only about a factor of two worse than estimates based on moderate-resolution follow-up spectra.

The use of a single continuum passband might lead to a correlation of KP with the colors of the stars, because the varying spectral energy distributions lead to a change in continuum slope, altering the line depth relative to a pseudo-continuum defined by the continuum band on the red side of the line only. However, in a plot of the residual of the KP measurements against  $B - V$ , we do not see any strong systematic effects of this sort (see lower panel of Fig. 3). This is probably due to the fact that the selection of metal-poor candidates is restricted to a

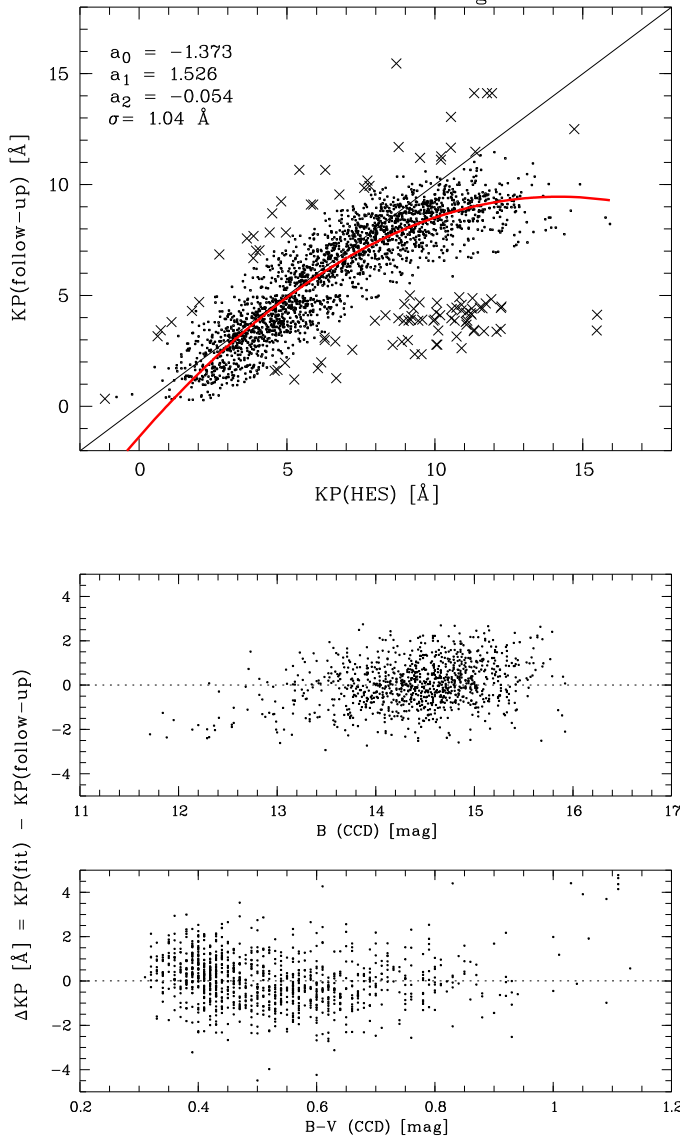


**Fig. 3.** Calibration of the KP index for the Ca II K line, using 2162 metal-poor stars from the HK survey present on HES plates. Stars that have been rejected from the fit as outliers are shown as crosses. As can be seen in the uppermost panel, the use of a broader line passband appears to lead to a later onset of saturation of the KP index compared to the follow-up spectra.

relatively narrow effective temperature range of approximately 4000–6600 K.

### 3.2.2. The GP index

For the measurement of the GP index from the HES spectra, we used continuum passbands covering 4246–4255 Å and 4446–4612 Å, and a 26 Å wide band centered on the bandhead of the G band (see Fig. 1).

The adopted calibration relation is a linear fit to 1990 data points. Measurements for 86 stars have been rejected as  $> 2\sigma$  outliers. The  $1-\sigma$  scatter of the GP measurements from the HES spectra around the fit is  $0.9$  Å, which would result in an uncertainty of  $\sim 0.2$  dex in  $[C/Fe]$  if other error sources are neglected (in particular, the errors in KP and color).

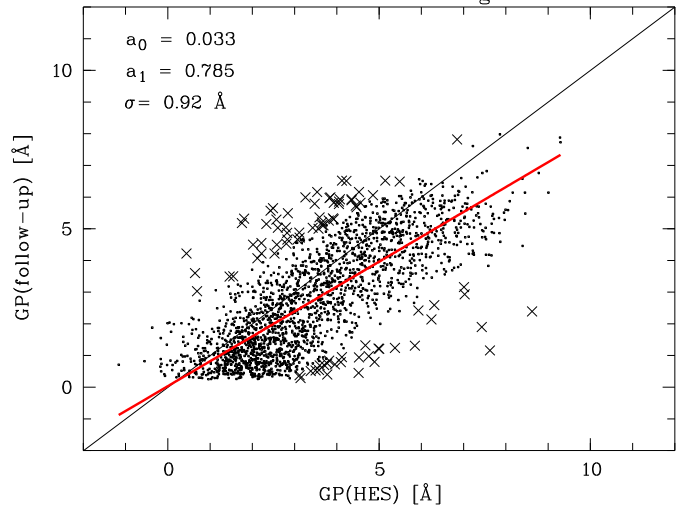


**Fig. 4.** Calibration of the GP index for the CH G band, using 2162 metal-poor stars from the HK survey present on HES plates. Stars that have been rejected from the fit as outliers are shown as crosses.

We emphasize that we *do not* involve GP in the selection of metal-poor candidates, but the index is useful for identifying candidate carbon-enhanced stars among the metal-poor candidates, if desired. For reference we list in Tab. A.1 estimates of  $[C/Fe]$  obtained for all HES metal-poor candidates, derived using the methods of Rossi et al. (2005). These estimates are based on measurements of the GP and KP indices from the HES spectra.

## 4. Selection of candidate metal-poor stars

In this section the procedures for selecting metal-poor candidates in the HES are outlined. We aim to develop a selection that (a) does not introduce an effective-temperature related bias, and that (b) restricts the selected stars to a manageable number of candidates for conducting medium-resolution spectroscopic follow-up observations, while maintaining a reasonable level of completeness. Since we are mainly interested in the most metal-poor stars, we target a completeness as high as possible for stars with  $[Fe/H] < -3.5$ , while some incompleteness at  $[Fe/H] \sim -3.0$  can be tolerated, and a rejection of as many stars with  $[Fe/H] > -2.5$  as possible is desired.

### 4.1. Selection criteria

#### 4.1.1. The $KP/(B-V)_0$ selection

The first of our selection criteria employs a cutoff line in the parameter space  $KP$  versus  $(B-V)_0$ . The measurements of  $B-V$  and  $KP$  from HES spectra have been discussed in Sections 3.1 and 3.2.1 above, respectively.

The reddening has been determined using the maps of Schlegel et al. (1998). By comparison of measured (dereddened)  $B-V$  colors with predictions of this color from the HP2 index for  $H\delta$ , measured in moderate-resolution spectra, Beers et al. (2002) found that at  $E(B-V) > 0.10$  the reddening of the Schlegel et al. maps is too high. That is,  $(B-V)_0$ , as computed from CCD  $B-V$  photometry and  $E(B-V)$  from the Schlegel et al. maps is systematically too blue for stars with  $E(B-V) > 0.10$  compared to the predictions of  $(B-V)_0$  from HP2. This problem was previously recognized by Arce & Goodman (1999). To



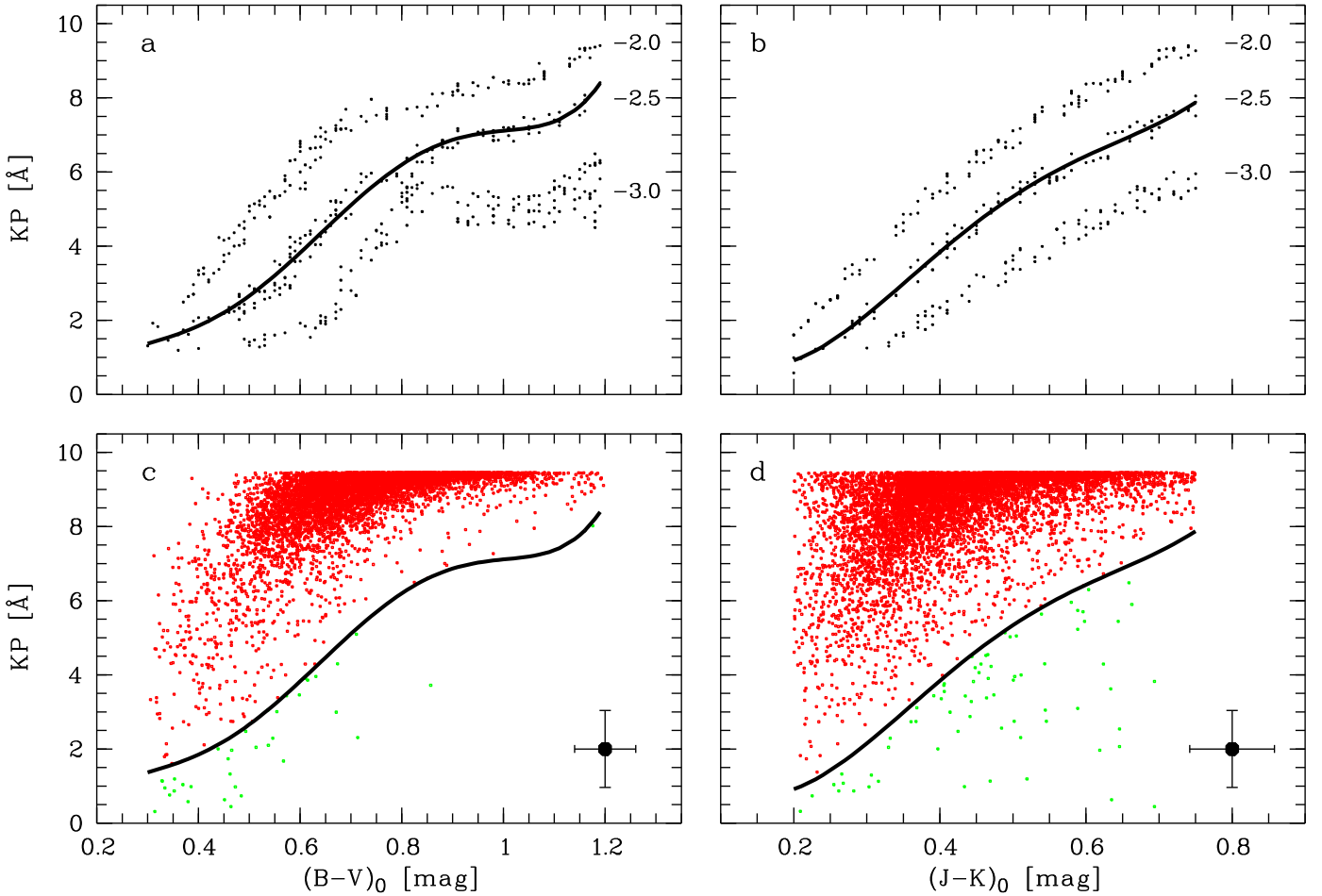


**Fig. 5.** Determination of cutoff lines for selecting metal-poor candidates (panels *a* and *b*), and their application to all stars on HES plate #12073, ESO field 147 (panels *c* and *d*). In panels *a* and *b*, simulated stars with  $[\text{Fe}/\text{H}]$  within 0.1 dex of the indicated metallicities are shown. To the data points corresponding to stars of  $[\text{Fe}/\text{H}] = -2.5 \pm 0.1$ , a polynomial was fitted (thick black lines). In the lower panels, typical error bars of the measurements of the KP index and  $(B - V)_0$  color from the HES spectra, as well as the typical  $1\text{-}\sigma$  uncertainty of the 2MASS  $(J - K)$  color, are shown. The larger uncertainties of the  $(J - K)$  colors lead to more candidates below the selection cutoff compared to the selection in the  $\text{KP}/(B - V)_0$  parameter space. The sharp cut at  $\text{KP} \sim 9.5 \text{ \AA}$  is due to the fact that the KP index cannot exceed this value due to the calibration of that index described in Sect. 3.2.1. As can be seen in the uppermost panel of Fig. 3, the fitted calibration curve reaches a maximum at this value.

rectify it, Beers et al. (2002) reduced any reddening in excess of  $E(B - V) = 0.10$  by 35 %. We adopt the same procedure.

The KP cutoff line was defined in the following way. An artificial sample of 10,000 stars was created, by computing with a random number generator values of  $(B - V)_0$  equally distributed in the range  $0.3 \leq (B - V)_0 \leq 1.2$ , and values of KP equally distributed in the range  $0.0 < \text{KP} < 12$ . These pairs of values were then converted into  $[\text{Fe}/\text{H}]$ , using an improved version of the method of Beers et al. (1999), which involves more calibration stars (Beers et al., in preparation). All data points yielding  $[\text{Fe}/\text{H}] = -2.5 \pm 0.1$  were selected, and a polynomial of 5th order was fitted to these data points. The weight of the points at  $(B - V)_0 < 0.45$  and  $(B - V)_0 > 1.00$  was increased by a factor of 10 to improve the quality of the fit. The result is displayed in panel *a* of Fig. 5. The cutoff line nicely runs parallel to the lower edge in the KP distribution at a given color (i.e., the marginal distribution in KP). That is, the lines could alternatively have been determined empirically, using a cutoff-location algorithm as was employed by Wisotzki et al. (2000) for selecting UV-excess objects in the HES.

An object is selected as a metal-poor candidate if it falls into the color range  $0.3 \leq (B - V)_0 \leq 1.2$  (roughly corresponding to  $4000 \text{ K} < T_{\text{eff}} < 6600 \text{ K}$ ), and if its KP value is below the cutoff for the given  $(B - V)_0$ , but above a threshold for a significant detection of an emission line (see Sect. 4.1.3 for details). Further ingredients for the  $\text{KP}/(B - V)_0$  selection are the average  $S/N$  per pixel in the  $B_J$  band and in the  $\text{Ca II H}$  and  $\text{K}$  region. This aims at rejecting spectra that are too noisy for a sensible candidate selection. A candidate is rejected if (a) the average  $S/N$  per pixel in the  $B_J$  band is lower than 5/1, or if (b) the average  $S/N$  in the  $\text{Ca II H}$  and  $\text{K}$  region is lower than 5/1. The method for estimating the noise per pixel of the HES spectra has been described by Christlieb et al. (2001b).

Criterion (a) typically corresponds to a magnitude limit of  $B_J < 17.5$ , while criterion (b) results in a restriction to objects that are about 1 mag brighter in the  $B_J$  band. However, the magnitude limit varies considerably from plate to plate, depending critically on the conditions under which the plates were exposed (i.e., sky background level and seeing). Bright stars with (partly) saturated HES spectra can have a higher  $S/N$  at  $\text{Ca II H}$  and  $\text{K}$

compared to the average  $S/N$  in the  $B_J$  band, so that the  $S/N$  criterion (a) rejects the brightest (i.e.,  $B < 11\text{--}13$ , depending on plate quality) stars, while at the faint end only criterion (b) has an effect.

Finally, all candidates with spectra affected by an overlap, according to the automated overlap detection algorithm, are rejected.

#### 4.1.2. The $KP/(J - K)_0$ selection

A selection cutoff in the  $KP$  versus  $(J - K)_0$  parameter space has been determined analogous to the cutoff in the  $KP$  versus  $(B - V)_0$  parameter space, except that a polynomial of 4th order was fit, and equal weights were assigned to all data points. The result is shown in panel *b* of Fig. 5.

The  $J$  and  $K$  magnitudes for the HES stars were retrieved from the 2MASS All-Sky Data Release. The cross-correlation of the two catalogs was accomplished by adopting the closest 2MASS point source within a search box of  $5'' \times 5''$  as the matching object. We note that the  $1\text{-}\sigma$  uncertainty of the HES coordinates is the same as the uncertainty of the DSS-I plate solutions, which is smaller than  $1''$  for point sources (see, e.g., Veron-Cetty & Veron 1996). The 2MASS astrometry is even more accurate; i.e.,  $\sigma = 0.1''$  for sources brighter than  $K_S = 14$  (Skrutskie et al. 2006). We adopted a search box considerably larger than the combined uncertainties to be able to identify the corresponding 2MASS source even in case of HES objects suffering from  $5\text{-}\sigma$  astrometric errors. Over 99 % of the HES sources fulfilling the  $S/N$  criteria (a) and (b) listed above were successfully identified in 2MASS.

We only make use of  $J$  and  $K$  magnitudes which were labeled with the photometric quality flags “A”, “B”, or “C”, and which had their blend and contamination flags set to 1 (i.e., one component present only), and 0 (i.e., source not affected by any artifacts), respectively. Applying these quality criteria results in the rejection of the  $J$  and  $K$  magnitudes for about 1 % of the HES sources identified in 2MASS.

The  $J - K$  colors were de-reddened by adopting the relation  $E(J - K) = 0.535 \cdot E(B - V)$ , derived from Table 6 of Schlegel et al. (1998). Here,  $E(B - V)$  values in excess of 0.10 have been scaled down in the same manner as was done for the de-reddening of  $B - V$  (see Sect. 4.1.1).

We restrict the candidate selection to stars in the color range  $0.2 < (J - K)_0 < 0.75$ . The application of the  $KP$  cutoff, the  $S/N$  criteria, and the rejection of overlaps follows the same procedures as the  $KP/(B - V)_0$  selection described in the previous section.

#### 4.1.3. Non-detection of the $\text{Ca II K}$ line

For stars near the main-sequence turnoff, the  $KP$  cutoff lines shown in Fig. 5 approach levels comparable to the measurement uncertainty of  $KP$ . Therefore, even if a star would have no  $\text{Ca II K}$  line, it might be rejected because random noise might result in the measurement of a  $KP$  index above the cutoff for turnoff stars. Thus it is mandatory to relax the selection criteria for these stars. This is achieved by including stars into the candidate sample if their  $KP$  index is above the cutoff, but a  $\text{Ca II K}$  line is not significantly detected in the HES spectrum.

Figure 6 shows the  $1\text{-}\sigma$  detection limit of  $\text{Ca II K}$  for all overlap-free spectra belonging to the source types stars or bright on one randomly selected HES plate. As can be seen by comparing this figure with Fig. 5, the selection criterion is

considerably relaxed for faint or very bright turnoff stars compared to the  $KP$  cutoffs. However, for stars at  $(B - V)_0 \gtrsim 0.5$  or  $(J - K)_0 \gtrsim 0.3$ , the additional criterion does not have any effect, because the  $KP$  cutoff for the stars in this color range is higher than the  $1\text{-}\sigma$  detection limit of  $\text{Ca II K}$  at any magnitude; a star having a  $KP$  value corresponding to a  $1\text{-}\sigma$  detection of  $\text{Ca II K}$  would be selected anyway.

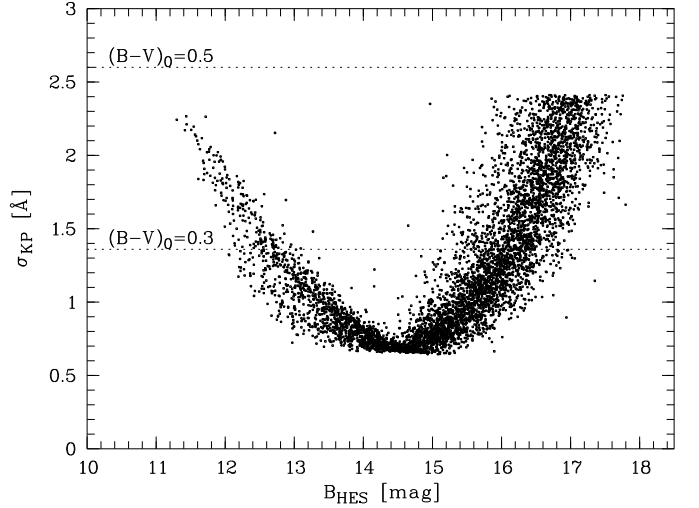


**Fig. 6.** The individual  $1\text{-}\sigma$  detection limit of  $\text{Ca II K}$  in HES spectra on HES plate #1528 (ESO field 894) as a function of the HES  $B$  magnitude. Overplotted are the selection cutoff lines for stars of  $(B - V)_0 = 0.3$  and  $0.5$  (dashed lines). The position of the lower line demonstrates that very bright or faint stars with  $(B - V)_0 = 0.3$  are rejected by the  $KP/(B - V)_0$  criterion even if a  $\text{Ca II K}$  line is not significantly detected (i.e.,  $\sigma_{KP}$  is larger than the cutoff value of  $KP$  in these cases); hence the selection needs to be relaxed in these cases, which is achieved with the  $\text{Ca II K}$  non-detection criterion (see Sect. 4.1.3). The position of the upper line shows that for stars  $(B - V)_0 \gtrsim 0.5$ , the selection does not have to be relaxed, because  $\sigma_{KP}$  is smaller than the cutoff value for stars in the whole magnitude range, and hence the  $\text{Ca II K}$  line is significantly detected in these cases.

To understand the behavior of the bright end of the curve shown in Fig. 6, one has to consider that the HES objective-prism plates are photographic plates that have been digitized with a microdensitometer. As one approaches the brightest magnitudes, and correspondingly high photographic densities of the objective-prism spectra, significantly lower numbers of photons pass through the photographic plate to be recorded by the scanner, thereby decreasing the  $S/N$  of the brighter HES spectra.

A star is selected if it falls into the color range  $0.2 < (J - K)_0 < 0.75$  or  $0.3 \leq (B - V)_0 \leq 1.2$ , and if  $\text{Ca II K}$  is not significantly detected in either absorption or emission. The last part of the criterion aims at rejecting dMe stars or other objects having  $\text{Ca II H}$  and  $\text{K}$  in emission. In addition, the same  $S/N$  criteria as in the  $KP/(B - V)_0$  and  $KP/(J - K)_0$  are applied, and spectra affected by overlaps are rejected.

#### 4.1.4. Application to the HES

Below we summarize the selection applied to each of the three HES source types.

**stars** (unsaturated point sources): An object is selected as a metal-poor candidate if it fulfills one or more of the criteria described in Sections 4.1.1–4.1.3 above; i.e., the  $KP/(B-V)_0$ ,  $KP/(J-K)_0$ , or the  $\text{Ca II K}$  non-detection criterion.

**bright** (bright sources above a saturation threshold): An object is selected as a metal-poor candidate if it either fulfills the  $KP/(J-K)_0$  criterion (Sect. 4.1.2) or the  $\text{Ca II K}$  detection criterion (Sect. 4.1.3), or both. We do not apply the  $KP/(B-V)_0$  criterion for the bright stars, because it has been shown by Frebel et al. (2006b) that the HES  $B-V$  colors are not reliable for the brightest stars due to saturation effects. Note, however, that the  $\text{Ca II K}$  non-detection criterion does involve the HES  $B-V$  color, but only for restricting the color range of the candidates to be selected.

**ext** (extended sources): All sources classified as extended are rejected to avoid contamination of the candidate sample with galaxies.

The application of the  $KP/(B-V)_0$  and  $KP/(J-K)_0$  criteria to all stars on one HES plate is illustrated in panels *c* and *d* of Fig. 5, respectively.

#### 4.2. Visual inspection

The candidates selected by the criteria described above have to be visually inspected to reject false positives caused, e.g., by emulsion flaws, scratches, dust, or other artifacts on the objective-prism plates, or by overlapping spectra that were not recognized by our automated procedures. We inspected the extracted HES spectrum together with the raw spectrum on the digitized objective-prism plate, as well as the corresponding regions on the relevant DSS-I direct plate.

To avoid any subjective selection biases during the visual inspection, only candidates were rejected that are clearly disturbed by artifacts or overlapping spectra, or clearly identifiable as “peculiar objects” (e.g., stars exhibiting  $\text{Ca II H}$  and  $\text{K}$  in emission, or other emission-line objects), galaxies, cool white dwarfs, etc. In Fig. 7 we show example spectra of such objects.

We also applied a subjective ranking of the candidates, by assigning them to one of the following classes: *mpca* – clearly no  $\text{Ca II K}$  line detected; *unid* – it is unclear whether a  $\text{Ca II K}$  line is detected; *mpcb* – a weak  $\text{Ca II K}$  line is detected; *mpcc* – a strong  $\text{Ca II K}$  line is detected. HES spectra of candidates classified in this way are shown in Fig. 8. This ranking is made for the specific purpose of prioritizing the follow-up spectroscopy target lists, allowing us to optimize the observational strategy. We emphasize that for statistical studies, such as determining the metallicity distribution function (MDF) of the Galactic halo, *complete* samples have to be compiled; i.e., *all* candidates selected on a given set of plates have to be followed up spectroscopically, regardless of their candidate class. Otherwise, non-quantifiable selection biases may result.

#### 5. Evaluation of the selection

We evaluated the selection of metal-poor candidates in the HES by means of a test sample of 1121 HK survey stars present on HES plates for which  $[\text{Fe}/\text{H}]$  has been determined based on moderate-resolution follow-up spectra, using an updated version of the methods of Beers et al. (1999). The test sample has been restricted to stars for which CCD  $B$  and  $V$  photometry exists, so that the evaluation is based on the most reliable  $[\text{Fe}/\text{H}]$  estimates. Furthermore, stars have been removed from the test sample if either the CCD  $V$  magnitude deviates by more than 1 mag from

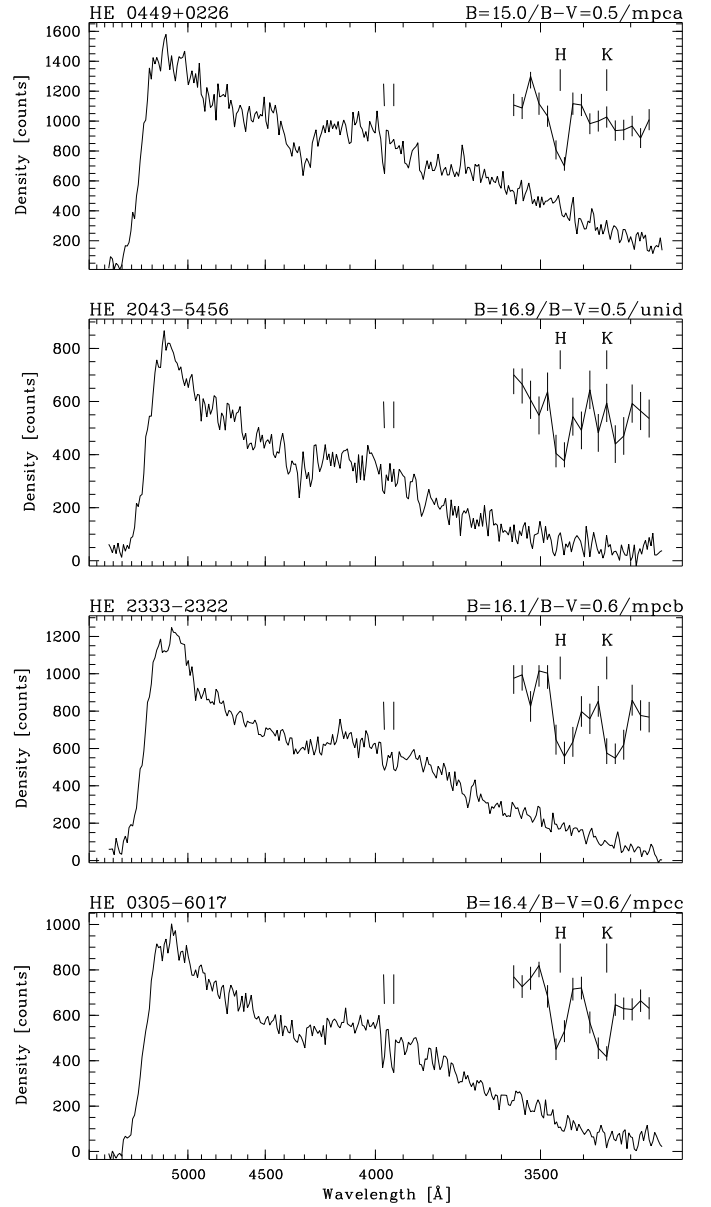


**Fig. 8.** HES example spectra of candidates of the classes *mpca*, *unid*, *mpcb*, *mpcc*. In the upper right corner of each panel, an enlargement of the  $\text{Ca II H}$  and  $\text{K}$  wavelength region is shown (note that  $\text{Ca II H}$  is blended with  $\text{H}\epsilon$ ).

the HES  $V$  magnitude, or if the CCD  $B-V$  color deviates from the HES  $B-V$  color by more than 0.5 mag. These stars are very likely mis-identifications of HK survey stars, resulting from the fact that a search box as large as  $15'' \times 15''$  was used during the cross-identification, since the HK survey coordinates can have uncertainties of more than 10 arcsec. The result of the evaluation of the selection is shown in Fig. 9.

In every candidate selection, there is a tradeoff between selection efficiency and completeness. Relaxed selection criteria lead to high completeness but lower efficiency (i.e., a higher number of false positives will contaminate the sample), while strict criteria lead to low completeness but high efficiency. Our evaluation of the selection shows that in the HES, a good compromise has been reached. While 738 of the 764 test sample stars at  $[\text{Fe}/\text{H}] > -2.0$  were rejected by the HES selection, resulting in a low number of false positives, a satisfac-



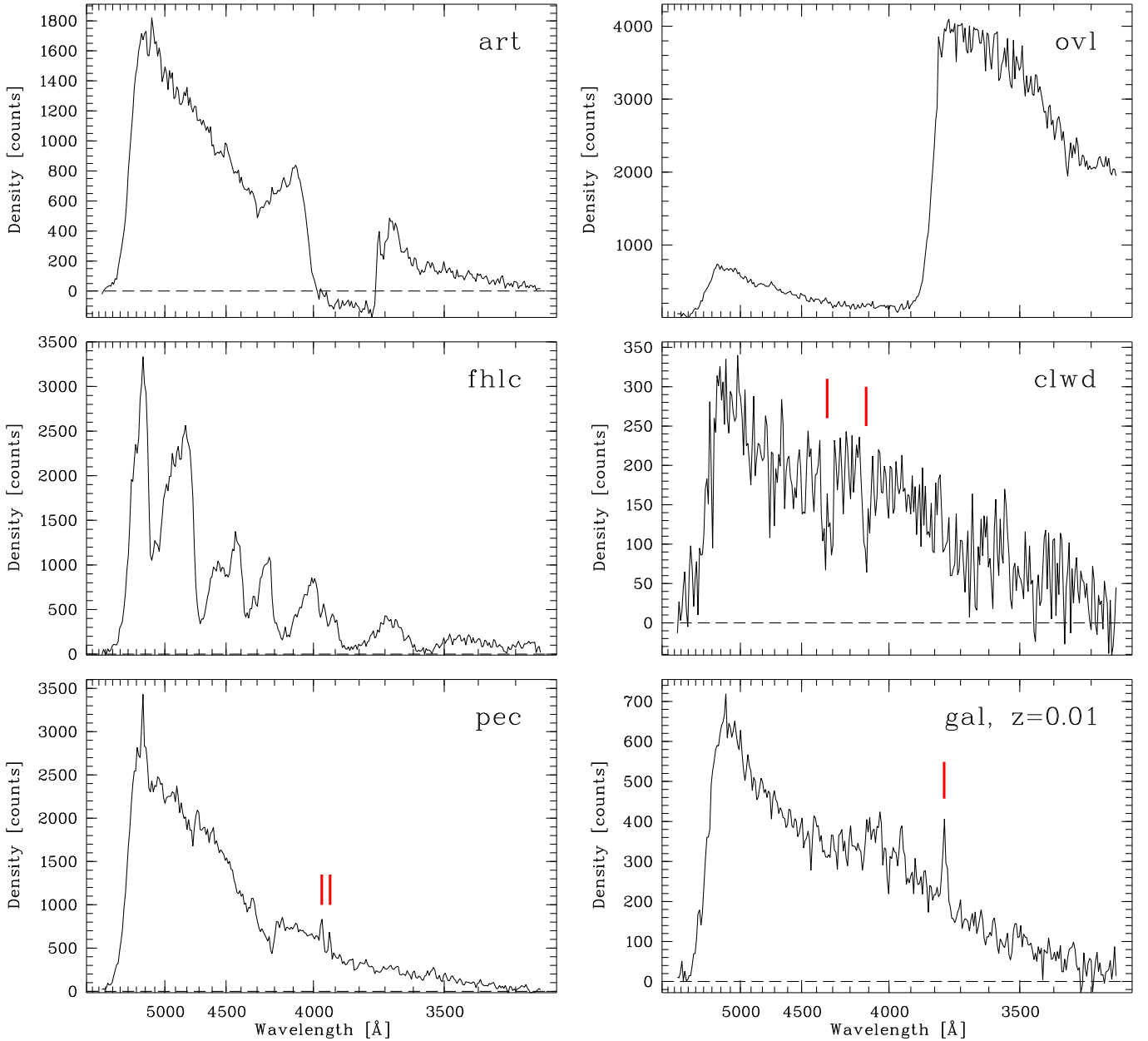


**Fig. 7.** HES example spectra of rejected metal-poor candidates. *art* – spectrum corrupted due to plate artifact, in this case by a scratch in the photographic emulsion; *ov1* – spectrum disturbed by bright object in dispersion direction, causing overlapping spectra; *fhlc* – faint high latitude carbon star; *clwd* – cool white dwarf, identifiable by the very broad lines of H $\gamma$  and H $\delta$  as well as the weak Balmer jump; *pec* – peculiar star (Ca II H and K in emission); *gal* – galaxy, showing [OII] 3727 Å in emission and at a redshift of  $z = 0.01$ .

tory level of completeness at the low-metallicity end is maintained: 20 of the 37 stars with  $[\text{Fe}/\text{H}] < -3.0$  have been selected, and all four stars with  $[\text{Fe}/\text{H}] < -3.5$  have been recovered. Here,  $[\text{Fe}/\text{H}]$  refers to the value that was determined from moderate-resolution follow-up spectra. These four stars are HE 0005–3547 = CS 22876-032 (Molaro & Castelli 1990), with  $[\text{Fe}/\text{H}] = -3.7$  (Norris et al. 2000); the bright ( $B_{\text{HES}} = 12.9$ ) star HE 0044–3755 = CD  $-38^\circ 245$  (Bessell & Norris 1984) = CS 22188-048, with  $[\text{Fe}/\text{H}] = -4.0$  (Norris et al. 2000; François et al. 2003); HE 0305-5442 = CS 22968-014, with  $[\text{Fe}/\text{H}] = -3.6$  (Cayrel et al. 2004); and HE 2356-0410 = CS 22957-027, with  $[\text{Fe}/\text{H}] = -3.4$  (Norris et al. 1997). The

quoted iron abundances were derived from high-resolution spectra.

## 6. Results

Application of the selection criteria to all 379 HES fields yielded 26,928 raw candidates, of which 5668 were rejected during the visual inspection. The largest fraction of them are stars which are clearly too hot (i.e., hotter than the main-sequence turnoff of old, metal-poor halo stars;  $T_{\text{eff}} \sim 6800$  K), as judged from the strength of the Balmer lines (1478 stars), followed by sources having HES spectra corrupted by plate artifacts (693 objects) or overlapping spectra (574 objects). Another 947 raw candidates

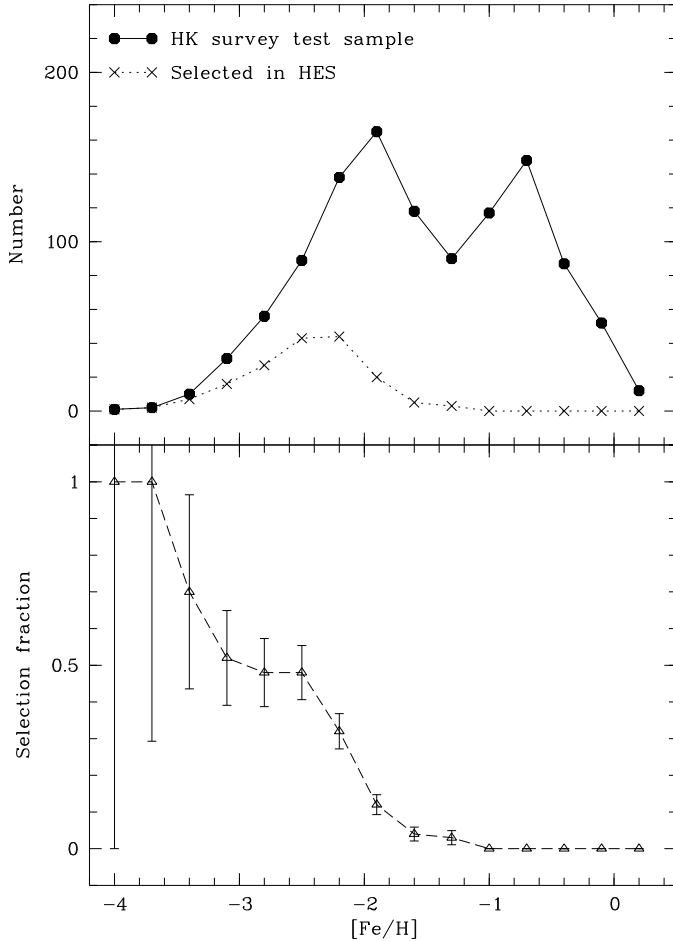


**Fig. 9.** HES selection fractions relative to a test sample of 1121 HK-survey stars present on HES plates.

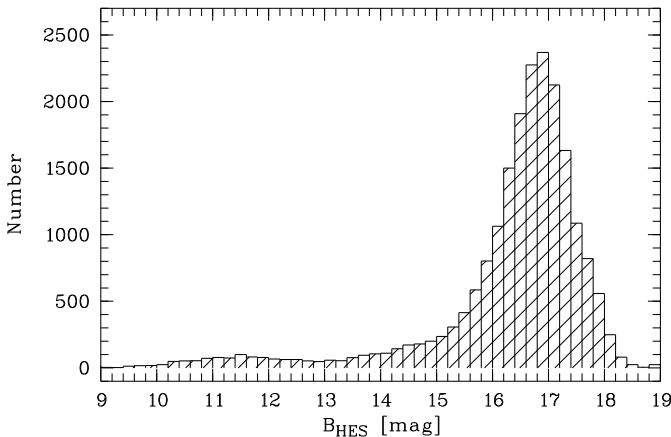


**Fig. 10.**  $B$  magnitude distribution of the accepted HES candidates.

were present on more than one plate quarter or on more than one field. The corresponding 989 multiple entries in the candidate list were removed. In total, we are left with 20,271 accepted candidates, which are listed in Tab. A.1. This corresponds to a surface density of 3 candidates per square degree.

In Tab. A.2 we provide the results of a cross-identification of the HES candidates with the visually-selected candidates from the HK survey (Beers et al. 1985, 1992; HK-I) as well as with

the lists of high-proper-motion stars of Ryan & Norris (1991) and Carney et al. (1994).

The magnitude distribution of the accepted HES candidates is shown in Fig. 10. We define the magnitude limit of a survey as the “point of half height” of the faint end of the magnitude distribution; i.e., the magnitude at which the number of objects per magnitude bin has dropped to half the maximum number of objects per magnitude bin of the distribution. When adopting this definition, the magnitude limit of the HES for metal-poor stars is  $B = 17.2$ . For comparison, the corresponding magnitude limit of the HK survey, as judged from 2267 HK survey stars present on HES plates, is  $B = 15.2$ .

Tab. 2 summarizes the number of stars in each candidate class, as well as the number of stars selected by each of the three selection criteria. From these numbers we conclude that the  $KP/(J - K)_0$  criterion is by far the most “relaxed” one, since in each of the four candidate classes at least 70 % of the candidates have been selected by this criterion.

**Table 2.** Number of stars in each candidate class and selected by each of the three selection criteria. The sum of the numbers in rows 1–3 in each column disagree with the total listed in row 4, because stars can be selected by more than one criterion.

Criterion	Candidate class				Total
	mpca	unid	mpcb	mpcc	
$KP/(B - V)_0$	406	1409	4496	2983	9294
$KP/(J - K)_0$	600	1840	7052	6663	16155
Ca II K non-detection	369	1222	2717	1481	5789
Total	772	2533	8872	8094	20271

Preliminary results of the spectroscopic follow-up observations indicate that the subset of candidates selected by the  $KP/(J - K)_0$  criterion contains a significantly higher number of false positives than the subsets selected by the other criteria; in particular, a considerable number of stars that are too blue. Tests suggest that this can largely be rectified by accepting only candidates having  $(J - K)_0 > 0.2$  and  $(B - V)_0 > 0.3$ . It appears that the use of the de-reddened  $J - K$  color alone is not very efficient in rejecting the bluer stars, probably due to the fact that the  $1-\sigma$  uncertainty of the 2MASS  $K$  magnitudes typically exceeds 0.1 mag for stars fainter than  $V = 16$ .

## 7. Conclusions

The high-quality digitization and accurate calibration of the photographic HES plates made it possible to perform a quantitative selection of candidate metal-poor stars, yielding 20,271 objects. The HK survey of Beers, Preston, and Shectman paved the way for our efforts. In particular, we employed HK survey stars present on HES plates for the calibration of the line indices and the  $B - V$  colors measured from HES spectra. For fixing the positions of the selection cutoff lines in color versus KP index parameter space, we rely on the techniques of Beers et al. (1999) for determination of  $[Fe/H]$  from the aforementioned observables. The work of Beers et al. (1999) in turn is based on medium-resolution spectroscopy of thousands, and high-resolution spectroscopy of hundreds of stars from the HK survey.

One of the advantages of a quantitative candidate selection is that the selection function is well-defined. That is, for any point in the color versus KP index parameter space, one can compute by means of simulations the probability that an object would be selected as a candidate, given the measurement uncertainties of

the relevant observational quantities. A precise knowledge of the selection function is important e.g. for statistical studies like determining the halo MDF, because one needs to understand how the candidate selection modifies the shape of the MDF. Such simulations, as well as an attempt to determine the halo MDF from a sample of HES stars for which follow-up observations already exists, are in progress (Schörck et al., in preparation).

Judging from a test sample of 1121 HK survey stars present on HES plates, the candidate selection in the HES is very efficient in rejecting stars with  $[\text{Fe}/\text{H}] > -2.0$ , while at the same time the HES sample is highly complete at the lowest metallicities. However, the result that 100 % of the test sample stars with  $[\text{Fe}/\text{H}] < -3.5$  were recovered in the HES is based on small number statistics (i.e., only 4 stars). Hence it is desirable to extend the test sample in the future, e.g. with metal-poor stars to be identified in the Southern Sky Survey (Keller et al. 2007).

Due to the fainter magnitude limit of the HES compared to the HK survey (i.e.,  $B = 17.2$  compared to  $B = 15.2$ ), the survey volume for metal-poor stars was extended by a factor of  $\sim 10$  compared to the HK survey. Hence, it was possible to identify in the HES objects which are too rare to be found with the HK survey; e.g., stars at  $[\text{Fe}/\text{H}] < -5.0$ . The fainter HES limit also allows one to explore outside the inner halo, which Carollo et al. (2007) have argued possesses a MDF that differs from that of the outer halo. The inner halo, according to these authors, has a peak metallicity ( $[\text{Fe}/\text{H}] = -1.6$ ) that is about a factor of three higher than that of the outer halo ( $[\text{Fe}/\text{H}] = -2.2$ ).

In our spectroscopic follow-up observations we mainly focus on the best (i.e., candidates assigned to classes *mpca* and *unid*) and brightest (i.e.,  $B < 16.5$ ) candidates. We have also endeavored to complete the observations in a few selected fields for statistical studies, such as determining the shape of the low-metallicity tail of the halo MDF. The results will be presented in future papers.

There are too many HES candidates to be processed in the course of our collaborative efforts alone. We therefore encourage the community to obtain follow-up spectroscopy of candidates that have not yet been observed by us. A list of the candidates in need of observations is available on request from the first author.

*Acknowledgements.* We thank J.E. Norris for comments on an earlier version of this paper which resulted in considerable improvements. We are grateful to S.G. Ryan for providing us with an electronic version of Table 3 of Ryan & Norris (1991). This publication makes use of data products from the Two Micron All Sky Survey, which is a joint project of the University of Massachusetts and the Infrared Processing and Analysis Center/California Institute of Technology, funded by the National Aeronautics and Space Administration and the National Science Foundation. N.C. and D.R. acknowledge financial support from Deutsche Forschungsgemeinschaft through grants Ch 214/3 and Re 353/44. N.C. is a Research Fellow of the Royal Swedish Academy of Sciences supported by a grant from the Knut and Alice Wallenberg Foundation. A.F. is supported through the W.J. McDonald Fellowship of the McDonald Observatory. T.C.B. acknowledges partial funding for this work from grants AST 04-06784, AST 06-07154, AST 07-07776, and PHY 02-16873: Physics Frontier Center/Joint Institute for Nuclear Astrophysics (JINA), all awarded by the US National Science Foundation.

## References

- Aoki, W., Beers, T., Christlieb, N., et al. 2007, *ApJ*, 655, 492  
Aoki, W., Frebel, A., Christlieb, N., et al. 2006, *ApJ*, 639, 897  
Arce, H. & Goodman, A. 1999, *ApJL*, 512, L135  
Barklem, P., Christlieb, N., Beers, T., et al. 2005, *A&A*, 439, 129  
Beers, T. & Christlieb, N. 2005, *ARA&A*, 43, 531  
Beers, T., Drilling, J., Rossi, S., et al. 2002, *AJ*, 124, 931  
Beers, T., Flynn, C., Rossi, S., et al. 2007, *ApJ Suppl.*, 168, 128  
Beers, T., Preston, G., & Shectman, S. 1985, *AJ*, 90, 2089  
Beers, T. C., Preston, G. W., & Shectman, S. A. 1992, *AJ*, 103, 1987  
Beers, T. C., Rossi, S., Norris, J. E., Ryan, S. G., & Shefler, T. 1999, *AJ*, 117, 981  
Bessell, M., Christlieb, N., & Gustafsson, B. 2004, *ApJ*, 612, L61  
Bessell, M. & Norris, J. 1984, *ApJ*, 285, 622  
Bucciarelli, B., García Yus, J., Casalegno, R., et al. 2001, *A&A*, 368, 335  
Carney, B., Latham, D., Laird, J., & Aguilar, L. 1994, *AJ*, 107, 2240  
Carollo, D., Beers, T., Chiba, M., et al. 2007, *Nature*, 450  
Carretta, E., Gratton, R., Cohen, J., Beers, T., & Christlieb, N. 2002, *AJ*, 124, 481  
Cayrel, R., Depagne, E., Spite, M., et al. 2004, *A&A*, 416, 1117  
Christlieb, N., Beers, T., Barklem, P., et al. 2004a, *A&A*, 428, 1043  
Christlieb, N., Bessell, M., Beers, T., et al. 2002, *Nature*, 419, 904  
Christlieb, N., Bessell, M., & Eriksson, K. 2008, in preparation  
Christlieb, N., Green, P., Wisotzki, L., & Reimers, D. 2001a, *A&A*, 375, 366  
Christlieb, N., Gustafsson, B., Korn, A., et al. 2004b, *ApJ*, 603, 708  
Christlieb, N., Timothy C. Beers, Thom, C., et al. 2005, *A&A*, 431, 143  
Christlieb, N., Wisotzki, L., Reimers, D., et al. 2001b, *A&A*, 366, 898  
Clarke, C. & Bromm, V. 2003, *MNRAS*, 343, 1224  
Cohen, J., Christlieb, N., Beers, T., Gratton, R., & Carretta, E. 2002, *AJ*, 124, 470  
Cohen, J., Christlieb, N., McWilliam, A., et al. 2004, *ApJ*, 612, 1107  
Cohen, J., Christlieb, N., Qian, Y., & Wasserburg, G. 2003, *ApJ*, 588, 1082  
Cohen, J., McWilliam, A., Shectman, S., et al. 2006, *AJ*, 132, 137  
Cohen, J., Shectman, S., Thompson, I., et al. 2005, *ApJL*, 633, L109  
Depagne, E., Hill, V., Christlieb, N., & Primas, F. 2000, *A&A*, 364, L6  
François, P., Depagne, E., Hill, V., et al. 2003, *A&A*, 403, 1105  
Frebel, A., Aoki, W., Christlieb, N., et al. 2005, *Nature*, 434, 871  
Frebel, A., Christlieb, N., Norris, J., Aoki, W., & Asplund, M. 2006a, *ApJL*, 638, L17  
Frebel, A., Christlieb, N., Norris, J., et al. 2006b, *ApJ*, 652, 1585  
Frebel, A., Christlieb, N., Norris, J., et al. 2007a, *ApJL*, 660, L117  
Frebel, A., Norris, J., Aoki, W., et al. 2007b, *ApJ*, 658, 534  
Goswami, A., Aoki, W., Beers, T., et al. 2006, *MNRAS*, 372, 343  
Hayek, W., Wiesendahl, U., Christlieb, N., et al. 2008, *A&A*, in preparation  
Hewett, P. C., Foltz, C. B., & Chaffee, F. H. 1995, *AJ*, 109, 1498  
Jonsell, K., Barklem, P., Gustafsson, B., et al. 2006, *A&A*, 451, 651  
Keller, S., Schmidt, B., Bessell, M., et al. 2007, *PASP*, 24, 1  
Lucatello, S., Beers, T., Christlieb, N., et al. 2006, *ApJL*, 652, L37  
Lucatello, S., Gratton, R., Carretta, E., et al. 2003, *AJ*, 125, 875  
Molaro, P. & Castelli, F. 1990, *A&A*, 228, 426  
Norris, J., Christlieb, N., Korn, A., et al. 2007, *ApJ*, 670, 774  
Norris, J. E., Beers, T. C., & Ryan, S. G. 2000, *ApJ*, 540, 456  
Norris, J. E., Ryan, S. G., & Beers, T. C. 1997, *ApJ*, 489, L169  
Reimers, D. 1990, *The Messenger*, 60, 13  
Rhee, J. 2000, PhD thesis, Michigan State University, East Lansing  
Rossi, S., Beers, T., Sneden, C., et al. 2005, *AJ*, 130, 2804  
Ryan, S. & Norris, J. 1991, *AJ*, 101, 1835  
Schlegel, D., Finkbeiner, D., & Davis, M. 1998, *ApJ*, 500, 525  
Skrutskie, M. F., Cutri, R. M., Stiening, R., et al. 2006, *AJ*, 131, 1163  
Veron-Cetty, M.-P. & Veron, P. 1996, *A&A*, 115, 97  
Wisotzki, L., Christlieb, N., Bade, N., et al. 2000, *A&A*, 358, 77  
Wisotzki, L., Köhler, T., Groote, D., & Reimers, D. 1996, *A&AS*, 115, 227

## Appendix A: The catalog of candidate metal-poor stars

Tab. A.1 lists all 20,271 candidate metal-poor stars selected in the HES which were not rejected during the visual inspection. The table is made available only electronically. It contains the following columns:

hename	HE designation
HESid	Unique HES identifier
ra2000	Right ascension at equinox 2000.0
dec2000	Declination at equinox 2000.0
field	ESO-SERC field number
objtype	Object type (stars/bright)
BHES	Photographic $B$ magnitude
BminV	$B - V$ color, estimated from HES spectra
UminB	$U - B$ color, estimated from HES spectra
EBminV	$E(B - V)$
BV0mphps	$(B - V)_0$
JminK0	$(J - K)_0$
VminK0	$(V - K)_0$
sn_bj	$S/N$ in $B_J$ band
sn_CaHK	$S/N$ in Ca H and K region
KPHES	KP index, measured in HES spectrum
sigKP	1- $\sigma$ uncertainty of KP index
GPHEs	GP index, measured in HES spectrum
selCaKBminV0	KP/ $(B - V)_0$ selection flag
selCaKJminK0	KP/ $(J - K)_0$ selection flag
selnoCaK	Ca K non-detection selection flag
canclass	Candidate class (mpca/unid/mpcb/mpcc)
FEHK	[Fe/H] estimate based on $(B - V)_0$ and KPHES
FEHR	[Fe/H] estimate based on $(J - K)_0$ and KPHES
CFER	[C/Fe], based on GPHEs and KPHES

Comments on individual columns:

**hename:** The Hamburg/ESO survey name consists of the letters “HE”, the first four digits of the right ascension at equinox 1950.0, and the first four digits of the declination at equinox 1950.0.

**HESid:** The average distance between two objects detected in the HES is 1.7 arcmin, hence the HE name described above is often not capable of uniquely identifying HES sources; i.e., two or more HES sources have the same HE name. Therefore, an additional identifier was introduced, which consists of the first seven digits of the right ascension at equinox 2000.0, the first six digits of the declination at equinox 2000.0, the plate quarter (a, b, c, or d), and the HES plate number. Example: For HE 0107–5240, which is located on quarter c of plate 2052 and at coordinates  $\alpha = 01^{\text{h}}09^{\text{m}}29^{\text{s}}.1$ ,  $\delta = -52^{\circ}24'34''$ , the HESid is HE0109291m522434c2052.

**ra2000, dec2000:** The coordinates were derived from the DSS-I, and they are typically accurate to within 1 arcsec.

**BHES:** Photographic magnitude derived from DSS-I  $B_J$  plates. For conversion between  $B_J$  and Johnson  $B$ , we use the transformation  $B = B_J + 0.28 \cdot (B - V)$ , which is valid for main-sequence stars in the color range  $-0.1 < (B - V) < 1.6$  (Hewett et al. 1995). The  $B - V$  color is the one derived from the HES spectra. A comparison of  $B_{\text{HES}}$  with CCD  $B$  magnitudes, using 963 HK survey stars present on HES plates and of object type stars or bright, yields that the 1- $\sigma$  uncertainty of  $B_{\text{HES}}$  is 0.2 mag.

**EBminV:**  $E(B - V)$  color excess from the maps of Schlegel et al. (1998). Any reddening in excess of  $E(B - V) = 0.10$  was reduced by 35 %, following (Beers et al. 2002).

**BV0mphps:** De-reddened  $B - V$  color, where  $B - V$  has been estimated from HES spectra using the calibrations described in Sect. 3.1.

**JminK0:** The  $J$  and  $K$  magnitudes are from 2MASS.

**VminK0:**  $V$  was computed from the DSS-I  $B$  magnitudes and the  $B - V$  color derived from HES spectra;  $K$  is from 2MASS.

**sn\_bj:** Average  $S/N$  per pixel of the HES spectra in the  $B_J$  band.

**sn\_CaHK:** Average  $S/N$  per pixel of the HES spectra in the Ca H and K wavelength region.

**FEHK, FEHR:** Estimates are given only if the Ca II K line is detected at  $> 1 \sigma$  level in the HES spectrum.

Tab. A.2 (available electronically only) contains the names of 276 stars which were originally discovered in previous surveys for metal-poor stars and which were re-discovered in the HES.

HESid	Unique HES identifier
hename	HE designation
HKIname	HK-I identifier
othernames	Other names